SCIENCE CHINA
Technological Sciences

Special Topic: Mechanics of Micro-nanostructured Materials
•Article•

https://doi.org/10.1007/s11431-020-1584-6

Size effect of deformation nanotwin bundles on their strengthening and toughening in heterogeneous nanostructured Cu

YOU ZeSheng[1*], LUO ShuSen[2] & LU Lei[2*]

[1] *Herbert Gleiter Institute of Nanoscience, Nanjing University of Science and Technology, Nanjing 210094, China;*
[2] *Shenyang National Laboratory for Materials Science, Institute of Metal Research, Chinese Academy of Sciences, Shenyang 110016, China*

Received March 1, 2020; accepted March 27, 2020; published online May 11, 2020

Herein, we fabricated a heterogeneous nanostructured Cu with deformation nanotwin bundles (NTBs) embedded in a matrix of nanograins by means of dynamic plastic deformation at liquid nitrogen temperature. We conducted fracture mechanical measurements to investigate the effect of longitudinal length of the NTBs on their strengthening and toughening. Results suggest that an increase in the NTB length had a marginal influence on the tensile strength; however, it remarkably promoted both fracture initiation toughness and crack growth toughness. Longer NTBs are more effective not only in intrinsically enhancing crack tip plasticity by suppressing the strain localization and void nucleation but also in serving as crack bridges behind the crack front to extrinsically resist the fracture by shielding the crack tip.

fracture toughness, nanotwins, *J*-integral, size effect, toughening mechanism

Citation: You Z S, Luo S S, Lu L. Size effect of deformation nanotwin bundles on their strengthening and toughening in heterogeneous nanostructured Cu. Sci China Tech Sci, 2020, 63, https://doi.org/10.1007/s11431-020-1584-6

1 Introduction

Uniform nanostructured metallic materials with a characteristic microstructural length scale in the nanometer regime (<100 nm) usually exhibit extraordinarily high strength but, unfortunately, sacrifice tensile ductility and fracture toughness [1–5]. Over the past decade, there have been many attempts at promoting tensile ductility through engineering internal boundaries [6,7] or tailoring spatially heterogeneous or gradient microstructures at multiple scales [8–11]. On the contrary, although fracture toughness is invariably of primary concern for engineering applications [12], there is still a lack of investigations targeted at developing strategies to toughen nanostructured metals [4,5].

The inferior fracture resistance of materials with nanoscale incoherent boundaries arises from the reduction in work hardening, which stimulates strain localization, and from easy intergranular damage either through ductile void formation or by brittle decohesion [4,13–16]. Regarding these two aspects, coherent twin boundaries (TBs) at the nanometer scale are of unique advantage. The nanotwinned metals are not only strong but also ductile with considerable strain hardening [17–21]. Moreover, the TBs are resistant to direct micro-void nucleation because the stress concentration arising from impinged dislocations is readily relaxed via the various interactions between the dislocations and TBs [22]. *In-situ* transmission electron microscopy (TEM) observations and molecular dynamics simulations clearly demonstrate that nanotwins are effective barriers resisting crack extension [23–26]. Unfortunately, it is still a great challenge to fabricate fully nanotwinned metals sufficiently thick to measure the inherent fracture toughness.

In metals and alloys with low stacking fault energies and deformations at low temperatures and/or high strain rates, deformation twinning can readily introduce a certain volume fraction of nanotwins [27–30]. The deformation nanotwins in

*Corresponding authors (email: zsyou@njust.edu.cn; llu@imr.ac.cn)

bundles are rather strong because of their fine spacings [31]. In addition, they could also positively impact the fracture resistance, considering their considerable ductility and toughness. Qin et al. [32,33] were the first to assess the fracture toughness of heterogeneous nanostructured pure Cu with nanotwin bundles (NTBs), inside a nanograin matrix treated by dynamic plastic deformation (DPD). Recently, Luo et al. [16] more accurately evaluated the fracture toughness of the same Cu based on the *J*-integral method. Xiong et al. [34–36] examined the fracture properties of ANSI 316L stainless steel with NTBs in matrices of both nanograins and annealed coarse grains. It was demonstrated by these studies that the synergy of strength and fracture toughness was substantially enhanced by the nanotwins. A crack in such heterogeneous structures is advanced by microvoid nucleation and coalescence within the nanograin matrix, followed by the bypassing of NTBs, leaving them as ductile crack bridges [34]. The NTBs are eventually extracted, producing deep elongated dimples on the fracture surfaces [16,32]. Both the crack bridges and deep dimples associated with NTBs contribute to the enhanced fracture toughness [16,34].

These results imply that elongating the NTBs would further promote the toughening effect [32,34]; however, the NTB size and the nanograin matrix varied with DPD strain in those studies, as more nonequilibrium high angle grain boundaries were produced. Therefore, it is impractical to explore the size effect of NTBs on strengthening and toughening based on the samples of different strains. In this study, we adjusted the longitudinal length of the NTBs in pure Cu by controlling the initial annealed grain size prior to subjection to the same DPD treatment. The effect of the NTB length on fracture initiation and crack growth toughness is examined by elastic-plastic fracture mechanical assessment based on the *J*-integral resistance curve. We also scrutinize the fracture surfaces and crack tip microstructural evolution for different NTB sizes to reveal the underlying toughening mechanisms.

2 Experimental procedure

2.1 Sample preparation

To change the NTB size, high purity (99.995 wt.%) Cu rods were thermally annealed for different durations at 600°C to obtain equiaxed grains with distinctively different initial grain sizes. Figure 1 shows the grain orientation maps of three annealed coarse-grained Cu. The average grain sizes of the three samples are 30, 150, and 540 μm. The samples were then subjected to DPD treatment with a strain rate of 10^2–10^3 s^{-1} at liquid nitrogen temperature (LNT) [37], hereinafter referred to as DPD-Cu-A, DPD-Cu-B, and DPD-Cu-C, respectively. A total true strain accumulation of approximately 2.0 was accomplished by multiple compressions to a final thickness h_f of 4.2 mm. The true strain is defined as $\varepsilon_T=\ln(h_i/h_f)$, where h_i and h_f are the initial and final thicknesses, respectively.

2.2 Fracture toughness tests

For the fracture tests, miniaturized compact tension C(T) specimens with a width W of approximately 8.0 mm, thickness B of approximately 4.0 mm, and initial notch depth of 3.2 mm were machined from the DPD disks by electrical discharge machining (EDM). The crack propagation direction was parallel to the radial direction (RD) of the disk, whereas the crack plane was normal to the tangential direction (TD) and parallel to the compression direction. Limited by the specimen thickness, only this cracking orientation could be tested. The fracture specimens were further fatigue pre-cracked in tension-tension mode with a stress ratio of 0.1 and frequency of 2 Hz, until an initial total crack length, a_0, of approximately 4.0 mm (~0.5W) was acquired. Moreover, to suppress crack-front tunneling, grooves with a depth of approximately 0.4 mm (10%B) on both sides were machined along the crack plane by EDM [38].

The fracture tests were performed on an Instron 5848 mechanical testing machine under displacement control with a displacement rate of 0.1 mm min^{-1}. The load-line displacement was measured by a non-contact crack-opening displacement gauge, as described in detail in ref. [38]. The fracture resistance was evaluated by constructing all of the *J*-integral resistance (*J*-*R*) curves, namely, the variation of the *J*-integral as a function of crack extension (Δa), following the single-specimen procedure in the ASTM E1820 standard [38,39]. The crack length was measured by elastic compliance technique, with instantaneous compliance determined by partially unloading the specimen and recording the load-displacement curve [38]. The unloading displacement rate is −0.1 mm min^{-1}. The fracture tests were repeatedly performed, totaling three trials for each DPD Cu sample to guarantee reproductivity.

2.3 Uniaxial tensile tests

The mechanical properties were determined by tensile tests with dog-bone-shaped flat specimens machined from the DPD disks by EDM. The gauge cross section of the specimens was 2.0 mm×0.5 mm and gauge length was 5.0 mm. The specimens were mechanically ground and then electrochemically polished to remove the surface damage layer. The tensile tests were conducted on an Instron 5848 mechanical testing machine with a load capacity of 2.0 kN at room temperature (25°C) with an initial strain rate of 5×10^{-3} s^{-1}. A contactless MTS LX300 laser extensometer was applied to measure the tensile strain. For each DPD Cu sample, at least

three tensile tests were performed.

2.4 Microstructural characterization

The microstructure of the as-prepared DPD samples was characterized by scanning electron microscopy (SEM; FEI NanoSEM 430) under backscattering electron (BSE) mode. The cross-sectional microstructures were also examined by a TEM JEOL 2010 microscope, operated at 200 kV. The TEM specimens were prepared by twin-jet polishing in an electrolyte consisting of 25% alcohol, 25% phosphoric acid, and 50% deionized water at −10°C. The fracture surfaces were examined by SEM secondary electron imaging. The microstructural evolution ahead of the crack tip was characterized by electron backscattering diffraction (EBSD).

3 Results

3.1 Microstructure

Figure 2 shows the microstructural characterizations of the DPD Cu samples. The microstructure is rather heterogeneous

Figure 1 (Color online) Grain orientation maps obtained by electron backscattering diffraction for annealed coarse-grained Cu with different average grain sizes for DPD treatment. (a) 30 μm; (b) 150 μm; (c) 540 μm.

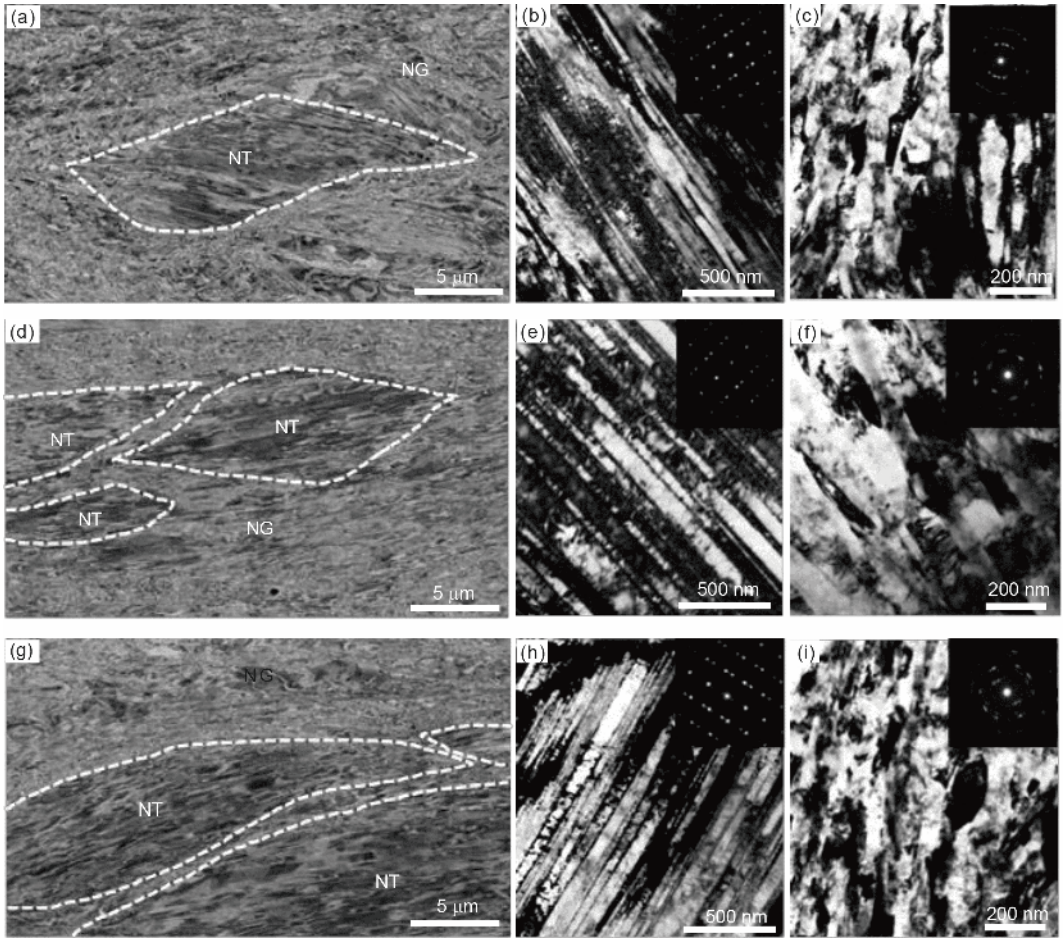

Figure 2 Characteristic microstructure of (a)–(c) DPD-Cu-A, (d)–(f) DPD-Cu-B, and (g)–(i) DPD-Cu-C samples. (a), (d), (g) SEM BSE micrographs showing heterogeneous microstructures with NTBs embedded in the nanograin matrix; (b), (e), (h) and (c), (f), (i) magnified TEM observations of the NTBs and nanograins, respectively. The insets in (b), (e), (h) and (c), (f), (i) are the corresponding selected area diffraction patterns. NT and NG represent nanotwins and nanograins, respectively.

with numerous bundles of nanoscale deformation twins (encircled by white dashes lines) embedded in a matrix of nanograins. All the TBs are roughly perpendicular to the DPD direction. The TEM micrographs of the NTBs in Figure 2(b), (e) and (h) show similar twin/matrix lamellae with a high density of accumulated dislocations in the three DPD Cu samples. The corresponding selected area electron diffraction (SAED) patterns demonstrate the twinning relationship. Figure 2(c), (f) and (i) show the analogous matrix, which consists of slightly elongated nanograins with aspect ratios of approximately 2.0 for the three DPD Cu samples. The nanograins are decorated with plenty of dislocations and randomly oriented, as demonstrated by the inserted SAED patterns.

Table 1 summarizes the microstructural parameters for all DPD Cu samples. The samples have almost identical twin thicknesses in the range of 44–47 nm in the NTBs and close transverse grain sizes in the range of 66–71 nm in the nanograin matrix. However, the longitudinal length and volume fraction of the NTBs are substantially different. For DPD-Cu-A, the average longitudinal length of the NTBs is 16±5 μm, and the volume fraction is only 15%. For DPD-Cu-B and C, the average longitudinal length increases to 31±1 and 84 ±5 μm, and the volume fraction is elevated to 32% and 35%, respectively. The large differences in the longitudinal length and volume of the NTBs are easy to understand, considering the microstructural evolution during DPD. When the copper is subjected to DPD at LNT, deformation twinning initially takes place, placing all of the grains in favorable orientations. As a consequence, the incipient deformation twins are much longer in DPD-Cu-C with larger grains than in DPD-Cu-A with smaller grains. The deformation twins are destroyed by localized shear bands and gradually evolve to nanograins when rotated to the plane normal to the compression direction with increasing DPD strain and become difficult to accommodate further uniform deformation. Additional shear bands are needed to shorten the longer deformation twins. Eventually, the remained NTBs are longer in the larger-grained DPD-Cu-C under the same DPD strain. Because the shear bands are initiated only when the nanotwin and dislocation structures are saturated and deformability-free, the dislocation densities of the nanograin matrix and of the NTBs of the three different samples are expected to be close in value.

3.2 Tensile properties

Figure 3 shows the typical engineering stress-strain curves for the DPD Cu and coarse-grained Cu for comparison. Table 2 summarizes the mechanical properties retrieved from the tensile tests. Clearly, both the 0.2% offset yield stress (σ_{ys}) and ultimate tensile stress (σ_{uts}) of the three DPD samples are much higher than those of the coarse-grained Cu. Nevertheless, the tensile ductilities are dramatically reduced, ow-

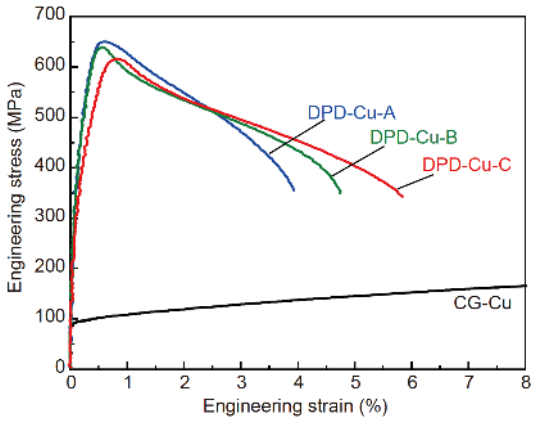

Figure 3 (Color online) Representative engineering stress-strain curves of DPD Cu and coarse-grained Cu.

Table 1 Microstructural parameters for the DPD Cu samples[a)]

Sample	Nanotwin bundles			Nanograins	
	λ (nm)	d_{NTB} (μm)	V_{NTB} (%)	d_{NG} (nm)	V_{NG} (%)
DPD-Cu-A	44±2	16±5	15	66±4	85
DPD-Cu-B	47±3	31±1	32	71±3	68
DPD-Cu-C	47±2	84±5	35	69±4	65

a) Parameters λ and d_{NTB} represent average twin thickness and average longitudinal length for the NTBs, respectively; V_{NTB} and V_{NG} represent volume fractions of the NTBs and nanograin matrix, respectively; d_{NG} represents average grain size for nanograins.

Table 2 Mechanical and fracture properties of the DPD Cu samples[a)]

Sample	σ_{ys} (MPa)	σ_{uts} (MPa)	δ_f (%)	J_{IC} (kJ m^{-2})	K_{IC} (MPa m$^{1/2}$)
DPD-Cu-A	601±8	650±10	4.0±0.8	11.7±0.9	39.3±1.3
DPD-Cu-B	593±6	637±9	5.0±0.6	17.4±2.1	47.9±2.4
DPD-Cu-C	582±7	626±11	6.9±0.3	27.6±2.9	60.3±3.1

a) σ_{ys}, 0.2% offset yield stress; σ_{uts}, ultimate tensile strength; δ_f, elongation to fracture; J_{IC}, 0.2 mm offset critical J-integral; K_{IC}, fracture toughness represented by critical stress intensity factor computed from J_{IC}.

ing to the diminished strain hardening capability and premature localized necking. For the three samples, there is only a slight reduction in σ_{uts} (from 650 MPa for DPD-Cu-A to 626 MPa for DPD-Cu-C) and a minor enhancement in the elongation to fracture (4.0% for DPD-Cu-A to 6.9% for DPD-Cu-C). Therefore, the uniaxial tensile properties of the DPD Cu are marginally affected by the variation in the microstructural constituents. The nanotwins are as strong as the nanograins, because both TBs and grain boundaries at the nanoscale effectively obstruct dislocation movement and cause similar strengthening [18].

3.3 Fracture toughness

Figure 4 shows the experimental force versus load-line displacement curves for the three DPD Cu samples. Different from the analogous uniaxial tensile response for the different microstructural compositions, the fracture behavior is significantly affected by the NTBs. For DPD-Cu-A, the force is dramatically reduced upon reaching the maximum value, which is an indication of the occurrence of catastrophic fracture. In contrast, for DPD-Cu-B and DPD-Cu-C, the force decreases gradually with increasing displacement, implying that the cracks in these two samples propagate in a more stable manner after initiation.

Based on the force-displacement data in Figure 4 and the instantaneous crack size determined by the elastic compliance method, the *J*-*R* curves are computed and shown in Figure 5. According to the ASTM E1820 standard [39], the maximum *J*-integral (J_{max}) that a specimen can measure is given by the smaller value of $B\sigma_Y/10$ and $b_0\sigma_Y/10$, where $\sigma_Y=(\sigma_{ys}+\sigma_{uts})/2$ is the average flow stress and $b_0=W-a_0$ is the initial size of the uncracked ligament. In addition, the maximum crack extension is limited by $\Delta a_{max}=0.25b_0$. As shown in Figure 5, all the *J*-integral values fall in the valid ranges (J_{max}=193 kJ m^{-2}, Δa_{max}=1 mm).

For DPD-Cu-B and DPD-Cu-C, the crack propagation is stable, and the *J*-integral increases with crack advancement. For such stable crack growth, a provisional *J*-integral, J_Q, is generally defined as the intersection point of the *J*-*R* curve with the 0.2 mm offset blunting line, $J=2\sigma_Y\Delta a$. Since DPD-Cu-A catastrophically breaks before reaching a crack extension of 0.2 mm, the *J*-integral value at the fracture is regarded as J_Q. Because the geometrical requirements for the *J*-dominance and plane strain state are fulfilled, namely, B, $b_0>10J_Q/\sigma_Y$ (approximately 0.5 mm for DPD Cu), all the J_Q values are size-independent plane strain fracture toughness, J_{IC}. The J_{IC} values can be converted to the critical stress intensity factor K_{IC} by the following relationship:

$$K_{IC}=\sqrt{\frac{EJ_{IC}}{1-\nu^2}}, \tag{1}$$

where the Young's modulus E and Possion's ratio ν are taken as 120 GPa and 0.3 for Cu, respectively. The average values of J_{IC} and K_{IC} for the three DPD Cu are tabulated in Table 2.

The fracture toughness K_{IC} is 39.3±1.3 MPa m$^{1/2}$ for DPD-Cu-A with an average NTB length of 16 μm. As the length of the NTBs increases to 31 μm, the K_{IC} value of DPD-Cu-B rises to 47.9±2.4 MPa m$^{1/2}$, and for DPD-Cu-C, with longer NTBs (84 μm), the K_{IC} value increases further to 60.3±3.1 MPa m$^{1/2}$. Considering the similar volume fractions of the NTBs and the significant difference in the K_{IC} values for DPD-Cu-B and DPD-Cu-C, we believe that the fracture resistance of the DPD Cu is controlled by the length of the NTBs, with the NTB volume playing a comparatively minor role.

In addition to the critical fracture initiation toughness, the NTB length also strongly impacts the crack growth resistance, as reflected by the higher slope of the *J*-*R* curve for DPD-Cu-C than for DPD-Cu-B and by the complete disappearance of the *J*-*R* curve behavior in DPD-Cu-A (Figure 5). The *J*-integral value is approximately 45 kJ m^{-2} ($K_{IC}\approx$ 77 MPa m$^{1/2}$) for DPD-Cu-C with a crack extension of 0.8 mm, whereas it is only approximately 25 kJ m^{-2} ($K_{IC}\approx$ 57 MPa m$^{1/2}$) for DPD-Cu-B with the same crack extension. It appears that the effects of NTBs on the fracture behavior during stable crack growth are far more significant than during fracture initiation.

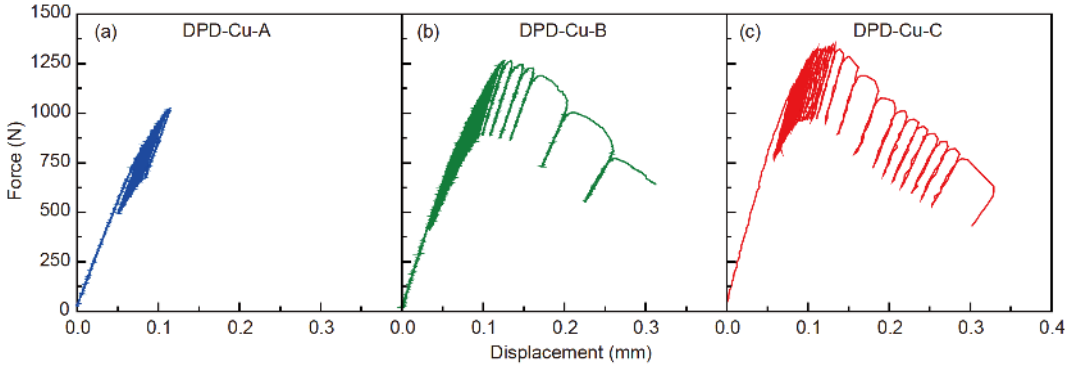

Figure 4 (Color online) Typical force versus load-line displacement curves for the three DPD Cu samples. (a) DPD-Cu-A; (b) DPD-Cu-B; (c) DPD-Cu-C.

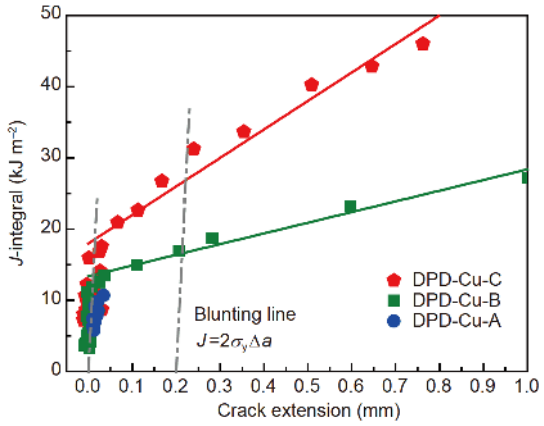

Figure 5 (Color online) *J*-integral resistance curves for the three DPD Cu samples.

3.4 Fractographic examination

The overall SEM fractographs of the different DPD Cu samples, Figure 6(a)–(c), apparently suggest that ductile fracture is the present mode of failure characterized by the formation of numerous dimples. The fracture morphologies are found to be rather heterogeneous with three different types of dimples (coarse/deep dimples, medium dimples, and fine/shallow dimples), in agreement with previous observations [16,32,34]. The coarse/deep dimples are magnified and displayed in Figure 6(d)–(f). Table 3 summarizes the statistical analysis on the dimple size for the three DPD samples. As expected, the average lengths of the coarse dimples (19 ±1, 30±2, and 97±5 μm for DPD-Cu-A, B, and C, respectively) are close to the corresponding longitudinal lengths of NTBs, and the area fractions of the coarse dimples are proportional to the volume fractions of the NTBs. Although the average grain size (~70 nm) in the nanograins is almost the same for the three samples, the mean diameter of the medium dimples associated with the fracture of the nanograins increases from 8±1 to 31±1 μm with increasing longitudinal NTB length. This suggests that the NTBs can suppress the micro-void nucleation in the nanograin matrix, which is discussed below. The fine dimples formed during the final extraction of the NTBs maintains the same size of 3 μm, whereas their area fraction increases from 9% to 20% from DPD-Cu-A to DPD-Cu-C, indicating that the affected zones of NTBs also increase with increasing NTB length.

4 Discussion

The fracture mechanical assessments clearly show that increasing the longitudinal length of the NTBs significantly enhances the fracture initiation and crack growth resistance. To better understand this phenomenon, the manner in which

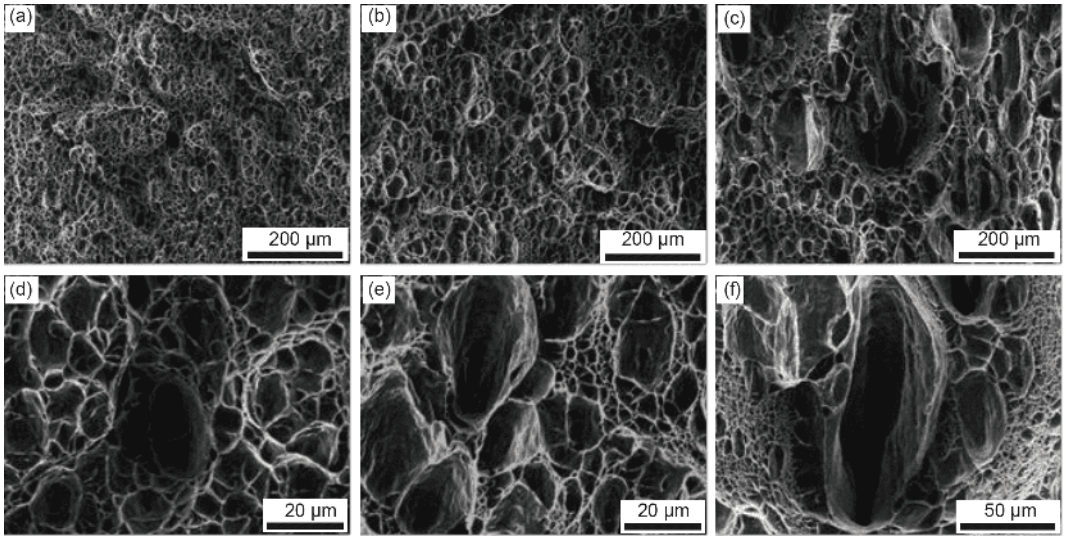

Figure 6 SEM observations on the fracture morphologies of the three DPD Cu samples. (a), (d) DPD-Cu-A; (b), (e) DPD-Cu-B; (c), (f) DPD-Cu-C.

Table 3 Average sizes and area fractions of the three types of dimples on the fracture surfaces of the three DPD Cu[a)]

Sample	Coarse dimples		Medium dimples		Fine dimples	
	D (μm)	*S* (%)	*D* (μm)	*S* (%)	*D* (μm)	*S* (%)
DPD-Cu-A	19±1	18%	8±1	73%	3±1	9%
DPD-Cu-B	30±2	28%	13±1	58%	3±1	14%
DPD-Cu-C	97±5	32%	31±1	48%	3±1	20%

a) *D*, dimple size; *S*, area fraction.

a crack is extended in homogeneous nanograined materials should be considered. Owing to the diminished strain-hardening capability, the plastic deformation around a crack tip in nanograined metals is expected to be localized into shear bands, rather than maintaining a uniform state [40]. Therefore, even with finite global crack tip plasticity, the local strain within the shear bands could be sufficiently high for void nucleation, preferentially at grain boundaries or triple junctions where strain incompatibility is intensified [41–43]. This premature damage evolution constrains the crack tip plasticity and results in fairly low fracture toughness in homogeneous nanocrystalline materials. In contrast, when NTBs are embedded, as schematically illustrated in Figure 7, once-localized shear bands that formed in the nanograin matrix propagate toward the NTB. Meanwhile, the more uniform deformation and higher strain-hardening of the nanotwins result in the arrest of the propagating shear bands. Consequently, the plastic strain within the arrested shear bands stops increasing and additional shear bands need to be initiated to accommodate further deformation within the nanograin matrix. These processes delocalize the concentrated strain and suppress or delay the nucleation and growth of the micro-voids, promoting the toughening of the fracture initiation.

The toughening is expected to be more effective for longer

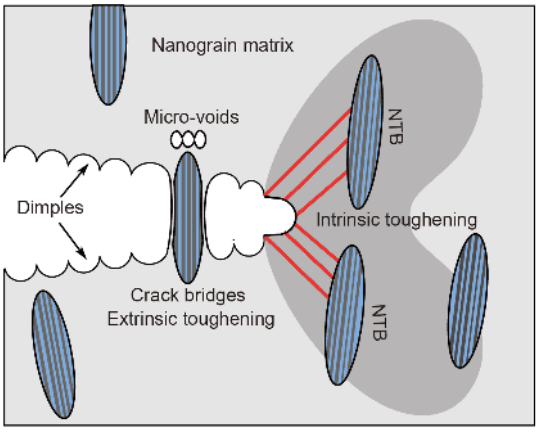

Figure 7 (Color online) Schematic illustration showing how the toughening effect of NTBs in heterogeneous nanostructured Cu can be considered in terms of intrinsic (resisting shear bands) and extrinsic (acting as crack bridges) toughening mechanisms.

NTBs owing to their significant size effect on fracture toughness. To further illustrate this point, fracture tests of DPD-Cu-A and DPD-Cu-C were interrupted nearly at the point of maximum force where the crack had just been extended a short distance; then, the specimens were bisected at the mid-thickness. Figure 8 shows the SEM examinations on the crack-tip deformation zone. For DPD-Cu-A with shorter

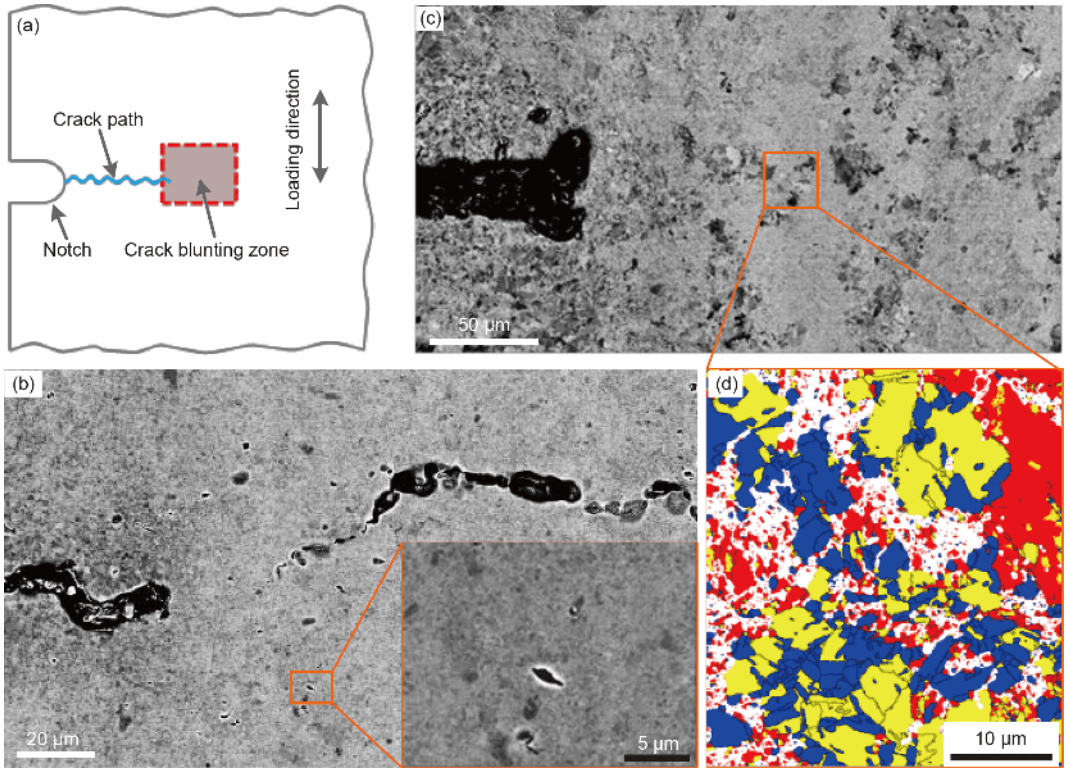

Figure 8 (Color online) Microstructural evolution ahead of the crack tip. (a) Schematic illustration of the loaded C(T) specimen showing the observation region. (b) SEM BSE observations for DPD-Cu-A with the inset indicating the formation of micro-voids. (c) SEM BSE observations for DPD-Cu-C showing many regions with significant grain growth. (d) EBSD map showing abnormal grain growth in a region far away from the crack tip (box in (c)). The blue and yellow regions represent the grain growth and dynamic recovery zones, respectively. The white and red regions stand for the as-deformed zone.

NTBs (Figure 8(b)), the crack tip is only blunted to a radius of approximately 5 μm. In front of the crack tip, a long crack, evidently reminiscent of nucleation and coalescence of micro-voids, emerged. Moreover, plenty of isolated micro-voids are also present in the deformation zone, with one typical micro-void of 3 μm length magnified, as shown in the inset of Figure 8(b). Except for the micro-crack and micro-voids, there is no evident microstructural change visible by the SEM observations. Therefore, we believe that the NTBs with an average length of 16 μm in DPD-Cu-A cannot effectively suppress the strain localization and micro-void nucleation in the nanograin matrix. It is likely that the localized shear bands transmit such small NTBs or migrate away from the gaps between the NTBs.

On the contrary, as shown in Figure 8(c), for DPD-Cu-C with longer NTBs, the crack tip is much more significantly blunted to a radius of 15 μm. There are no visible micro-voids or cracks ahead of the crack tip; however, the microstructure in the deformation zone is significantly coarsened. Figure 8(d) displays an EBSD pattern quality map of a region approximately 100 μm away from the crack tip. The blue regions are coarsened grains with diameters of several micrometers, whereas the yellow and red regions represent recovered and original nano-grains, respectively. The long NTBs effectively impede the strain localization in the nanograin matrix and make the GB migration operative, which releases the stress concentration arising from the strain incompatibility. Therefore, the formation of GB voids is completely arrested or delayed, resulting in much coarser dimples (31 μm for DPD-Cu-C versus 8 μm for DPD-Cu-A, see Table 3). In this manner, the NTBs play an essential role in promoting the fracture toughness, intrinsically elevating the plasticity of the nanograin matrix and, thus, dissipating more irreversible plastic energy.

In addition to improving the crack tip plasticity, the NTBs also serve as crack bridges in the wake of the crack front, as revealed by Xiong et al. [34], delaying fracture by shielding the crack tip [12]. The crack bridges develop because the easy void nucleation and coalescence extends the crack in advance through the nanograin matrix, causing it to pass around the NTBs, as shown in Figure 7. With further loading, the NTBs are eventually extracted entirely from the matrix [34]. Therefore, the longer the NTBs are, the more difficult it is to extract them, consuming more plastic work. Furthermore, such a toughening of the crack-tip shielding is proportional to the area of the uncracked bridging-ligaments between the crack surfaces. Since both coarse and fine dimples are related to the NTBs, their area fractions together represents the area fraction of crack bridges during fracture. According to Table 3, the area fraction of the nanotwin crack bridges increases from 27% for DPD-Cu-A to 52% for DPD-Cu-C. Consequently, the longer NTBs are beneficial to the enhancement of the extrinsic toughening arising from the nanotwin crack bridging and greater fracture surface tortuosity.

Apart from the intrinsic and extrinsic toughening effects discussed above, there are also other features associated with the reinforcement by NTBs. First, the flow strength of the nanotwins is comparable with or even higher than the nanograin matrix [31]. Consequently, the incorporation of more NTBs does not sacrifice the desirable strength. Second, both NTBs and the nanograin matrix are elastically and plastically compatible [12]. As mentioned above, the failure always takes place in the nanograin matrix, rather than directly along the boundaries between the NTBs and nanograin matrix. Furthermore, since the nanograin matrix at the deformed state is the weak link limiting the fracture resistance, further optimization in the strength and toughness combination is possible by controlled thermal treatment, which slightly modifies the grain boundary structures and increases the deformability. The strength might be slightly reduced; however, the gain in the fracture toughness is far more significant, as has been demonstrated recently in 316L stainless steel [34]. The unique toughening effect of the nanotwins indicates a new direction to optimize the combination of high strength and high damage tolerance by engineering the NTBs chemically (adjusting stacking fault energy) and thermo-mechanically.

5 Conclusions

To conclude, we generated heterogeneous nanostructured Cu containing a mixed structure of NTBs and nanograins by DPD at LNT. By adjusting the grain size of annealed Cu prior to subjection to the DPD treatment, we changed the longitudinal length of the NTBs from 16 to 84 μm, while maintaining the twin thickness constant. Tensile tests reveal similar high strengths (626–650 MPa), irrespective of the different NTBs. On the contrary, fracture mechanical experiments demonstrate a strong dependence of the fracture resistance on the NTB length. The critical fracture initiation toughness K_{IC} is only 39 MPa $m^{1/2}$ for NTBs, with an average length of 16 μm but remarkably increases to over 60 MPa $m^{1/2}$ for an average NTB length of 84 μm. For the latter, the crack growth toughness is also remarkably elevated. Intrinsically, the longer NTBs more effectively suppress the strain localization in the nanograin matrix and enhance the crack tip plasticity. Extrinsically, the longer NTBs promote toughening of the crack-tip shielding by acting as crack bridges behind the crack front. These findings demonstrate the feasibility of toughening nanostructured metallic materials without sacrificing the desirable high strength by controlling the nanotwins.

You Ze-Sheng was supported by the National Key R&D Program of China (Grant No. 2017YFA0204403). Lu Lei acknowledges financial support from

the National Natural Science Foundation of China (Grant Nos. U1608257 and 51931010), the Key Research Program of Frontier Science and the International Partnership Program (Grant No. GJHZ2029), Chinese Academy of Sciences, and Liaoning Revitalization Talents Program (Grant No. XLYC1802026).

1 Lu K. The future of metals. Science, 2010, 328: 319–320
2 Meyers M A, Mishra A, Benson D J. Mechanical properties of nanocrystalline materials. Prog Mater Sci, 2006, 51: 427–556
3 Zhu Y T, Liao X. Retaining ductility. Nat Mater, 2004, 3: 351–352
4 Pippan R, Hohenwarter A. The importance of fracture toughness in ultrafine and nanocrystalline bulk materials. Mater Res Lett, 2016, 4: 127–136
5 Pineau A, Amine Benzerga A, Pardoen T. Failure of metals III: Fracture and fatigue of nanostructured metallic materials. Acta Mater, 2016, 107: 508–544
6 Lu K. Stabilizing nanostructures in metals using grain and twin boundary architectures. Nat Rev Mater, 2016, 1: 16019
7 Lu K, Lu L, Suresh S. Strengthening materials by engineering coherent internal boundaries at the nanoscale. Science, 2009, 324: 349–352
8 Wu X, Zhu Y. Heterogeneous materials: A new class of materials with unprecedented mechanical properties. Mater Res Lett, 2017, 5: 527–532
9 Wu X, Yang M, Yuan F, et al. Heterogeneous lamella structure unites ultrafine-grain strength with coarse-grain ductility. Proc Natl Acad Sci USA, 2015, 112: 14501–14505
10 Wu X L, Jiang P, Chen L, et al. Synergetic strengthening by gradient structure. Mater Res Lett, 2014, 2: 185–191
11 Lu K. Making strong nanomaterials ductile with gradients. Science, 2014, 345: 1455–1456
12 Ritchie R O. The conflicts between strength and toughness. Nat Mater, 2011, 10: 817–822
13 Kumar K S, Suresh S, Chisholm M F, et al. Deformation of electrodeposited nanocrystalline nickel. Acta Mater, 2003, 51: 387–405
14 Hohenwarter A, Pippan R. Fracture toughness evaluation of ultrafine-grained nickel. Scripta Mater, 2011, 64: 982–985
15 Luo S, You Z, Lu L. Thickness effect on fracture behavior of columnar-grained Cu with preferentially oriented nanoscale twins. J Mater Res, 2017, 32: 4554–4562
16 Luo S S, You Z S, Lu L. Intrinsic fracture toughness of bulk nanostructured Cu with nanoscale deformation twins. Scripta Mater, 2017, 133: 1–4
17 You Z S, Lu L, Lu K. Tensile behavior of columnar grained Cu with preferentially oriented nanoscale twins. Acta Mater, 2011, 59: 6927–6937
18 Shen Y F, Lu L, Lu Q H, et al. Tensile properties of copper with nanoscale twins. Scripta Mater, 2005, 52: 989–994
19 Lu L, Shen Y, Chen X, et al. Ultrahigh strength and high electrical conductivity in copper. Science, 2004, 304: 422–426
20 Lu L, You Z S, Lu K. Work hardening of polycrystalline Cu with nanoscale twins. Scripta Mater, 2012, 66: 837–842
21 Dao M, Lu L, Shen Y F, et al. Strength, strain-rate sensitivity and ductility of copper with nanoscale twins. Acta Mater, 2006, 54: 5421–5432
22 You Z, Lu L. Deformation and fracture mechanisms of nanotwinned metals. Natl Sci Rev, 2017, 4: 519–521
23 Shan Z W, Lu L, Minor A M, et al. The effect of twin plane spacing on the deformation of copper containing a high density of growth twins. JOM, 2008, 60: 71–74
24 Zeng Z, Li X, Lu L, et al. Fracture in a thin film of nanotwinned copper. Acta Mater, 2015, 98: 313–317
25 Kim S W, Li X, Gao H, et al. *In situ* observations of crack arrest and bridging by nanoscale twins in copper thin films. Acta Mater, 2012, 60: 2959–2972
26 Shin Y A, Yin S, Li X, et al. Nanotwin-governed toughening mechanism in hierarchically structured biological materials. Nat Commun, 2016, 7: 10772
27 Lu K, Yan F K, Wang H T, et al. Strengthening austenitic steels by using nanotwinned austenitic grains. Scripta Mater, 2012, 66: 878–883
28 Tao N R, Lu K. Nanoscale structural refinement via deformation twinning in face-centered cubic metals. Scripta Mater, 2009, 60: 1039–1043
29 Li Y S, Tao N R, Lu K. Microstructural evolution and nanostructure formation in copper during dynamic plastic deformation at cryogenic temperatures. Acta Mater, 2008, 56: 230–241
30 Bouaziz O, Barbier D, Cugy P, et al. Effect of process parameters on a metallurgical route providing nano-structured single phase steel with high work-hardening. Adv Eng Mater, 2012, 14: 49–51
31 Zhang Y, Tao N R, Lu K. Mechanical properties and rolling behaviors of nano-grained copper with embedded nano-twin bundles. Acta Mater, 2008, 56: 2429–2440
32 Qin E W, Lu L, Tao N R, et al. Enhanced fracture toughness and strength in bulk nanocrystalline Cu with nanoscale twin bundles. Acta Mater, 2009, 57: 6215–6225
33 Qin E W, Lu L, Tao N R, et al. Enhanced fracture toughness of bulk nanocrystalline Cu with embedded nanoscale twins. Scripta Mater, 2009, 60: 539–542
34 Xiong L, You Z S, Qu S D, et al. Fracture behavior of heterogeneous nanostructured 316L austenitic stainless steel with nanotwin bundles. Acta Mater, 2018, 150: 130–138
35 Xiong L, You Z S, Lu L. Fracture behavior of an austenitic stainless steel with nanoscale deformation twins. Scripta Mater, 2017, 127: 173–177
36 Xiong L, You Z S, Lu L. Enhancing fracture toughness of nanotwinned austenitic steel by thermal annealing. Scripta Mater, 2016, 119: 55–59
37 Tao N R, Lu K. Dynamic plastic deformation (DPD): A novel technique for synthesizing bulk nanostructured metals. J Mater Sci Technol, 2007, 23: 771–774
38 You Z, Qu S, Luo S, et al. Fracture toughness evaluation of nanostructured metals via a contactless crack opening displacement gauge. Materialia, 2019, 7: 100430
39 ASTM E1820-15. Standard test method for measurement of fracture toughness. American Society of Testing and Materials, Philadelphia (PA), 2015
40 Xie J, Wu X, Hong Y. Shear bands at the fatigue crack tip of nanocrystalline nickel. Scripta Mater, 2007, 57: 5–8
41 Farkas D, Van Swygenhoven H, Derlet P M. Intergranular fracture in nanocrystalline metals. Phys Rev B, 2002, 66: 060101
42 Hasnaoui A, Van Swygenhoven H, Derlet P M. Dimples on nanocrystalline fracture surfaces as evidence for shear plane formation. Science, 2003, 300: 1550–1552
43 Li H, Ebrahimi F. Ductile-to-brittle transition in nanocrystalline metals. Adv Mater, 2005, 17: 1969–1972
44 Yan F K, Tao N R, Archie F, et al. Deformation mechanisms in an austenitic single-phase duplex microstructured steel with nanotwinned grains. Acta Mater, 2014, 81: 487–500